AIAA 2000-4104
Forebody Aerodynamic Asymmetry on a Full-Scale F-15 Radome

Jacob Kay
John Ralston

Bihrle Applied Research Inc.
Hampton, VA

AIAA Aerodynamics and Flight Mechanics Conference and Exhibit
14-17 August 2000 / Denver, Colorado

FOREBODY AERODYNAMIC ASYMMETRY ON A FULL-SCALE F-15 RADOME

Jacob Kay *
John Ralston **
Bihrle Applied Research, Inc.
18 Research Drive, Hampton, Va. 23666
(757) 766-2416 FAX (757)766-9227

Abstract

A full-scale F-15 forebody wind tunnel test was conducted at the Langley Full Scale Tunnel. The goal of this program was to assess the impact of radome imperfections on the aerodynamic characteristics at high angles of attack. The results would support the possible revision of fleet F-15 radome maintenance requirements to prevent future high angle of attack departures associated with forebody side force and yawing moment asymmetry.

The force and moment data as well as the surface pressure measurement obtained in the wind tunnel indicated that a high angle of attack aerodynamic offset could be triggered by minute forebody surface anomalies. Small imperfections near the apex of the radome caused significant forebody flow asymmetry while gross repair patches and ridges further aft on the forebody had minimal effects. Specifically, the direction and magnitude of the aerodynamic offset were very sensitive to minute geometric anomalies on or near the radome nose cap. Further aft from the radome apex, significantly larger imperfections were required to produce the same offset. These data clearly demonstrated the development of forebody aerodynamic asymmetry is primarily a function of the imperfection's proximity to the apex of the forebody.

Introduction

Sub-scale high-angle-of-attack wind-tunnel testing on aircraft configurations with slender circular ogive forebodies have consistently revealed significant yawing moment and side force offsets at zero sideslip in the 50° to 70°α region (e.g., Ref. 1,through 4). Research efforts on sub-scale forebody flow characteristics at high angles of attack have demonstrated the aerodynamic sensitivity to small geometric conditions on the forebody (Ref. 5). More specifically, the sub-scale F-15 wind tunnel data collected for the Air Force's Keep Eagle Program in 1993 also indicated the F-15's tendency to exhibit directional bias at high angles of attack (Ref. 6). These results were confirmed in subsequent high angle of attack flight tests (Ref. 7). While these and other tests have been empirically correlated to results observed in flight, questions relative to the applicability of sub-scale test results to full-scale aircraft have persisted; i.e., if offsets are observed in subscale laminar flow conditions, will they be reproduced at full scale Reynolds numbers where fully turbulent flow conditions exist?

In 1995, a nose-slice departure following an abrupt full aft-stick input for a symmetrically loaded F-15C was reported at Nellis AFB. Observed irregular radome conditions were suspected to be the cause of the aerodynamic anomaly that led to the incident. Following the replacement of the radome, the aircraft demonstrated acceptable high angle of attack behavior. This prompted an investigation into the F-15's high angle of attack forebody aerodynamic characteristics at the Langley Full Scale Tunnel using the actual full-scale radomes.

Prior to the wind tunnel entry, McDonnell Douglas had conducted a survey on the F-15 forebody conditions to identify surface imperfections sustained by the radomes in their operational environment. With such information, the wind tunnel test program was to assess the forebody imperfections' impact on the F-15's high angle of attack aerodynamic characteristics. These activities supported the formulation of radome/forebody maintenance requirements to minimize future occurrence of departure associated with forebody aerodynamic asymmetry.

Nomenclature

The units of physical quantities used herein are represented in U.S. Customary Units, unless otherwise noted.

AOA	angle of attack, deg.
AOS	angle of sideslip, deg.
b	wing span, ft.
c	mean aerodynamic chord, ft.
Cn	yawing moment coefficient.
Cp	pressure coefficient.
FS	fuselage station, in.
MAC	mean aerodynamic chord, ft.
Q	dynamic pressure, psf.

* Senior Aerospace Engineer
** Engineering Manager

S	wing area, ft^2
α	angle of attack, deg.
β	angle of sideslip, deg.

Subscripts:

local	local surface.
∞	free stream.

Test Description

Radomes

Production F-15 radomes were provided by the Air Force for the forebody test. One radome had the rain erosion boot (a rubber cover that extended from the nose tip aft for approximately 12 inches) removed and was configured with a series of flush pressure taps for surface pressure measurements. A total of 192 pressure ports were installed on the surface of the radome. Six rings of thirty-two pressure ports were installed at FS 120.3, 124.3, 129.3, 141.3, 165.3 and 189.3. The radial distribution of the pressure ports was designed such that finer resolution along the sides of the forebody cross section could capture the surface pressure gradient associated with flow separation.

All current F-15 radomes are configured with a metal nose cap at the apex of the nose. The 1.5-in diameter by 0.75-in tall circular stainless steel cap is attached to the apex of the radome and over the end of the rain erosion boot to minimize deterioration to the radome apex during flight. In addition to the painted caps attached to the fleet radomes used, the Air Force provided five additional used caps and MDA supplied a new unpainted cap for testing

A full-scale afterbody model was constructed for the section between FS 207.65 and FS 261.266 to function as a mounting interface between the radome and the balance block and to extend the effective length of the test article. This resulted in a 12-ft forebody model when mated to a production radome. The balance block attachment point was located such that the axis of the NASA Langley's VST-11 balance was located on BL 0.0 and WL116.173 and its moment center on FS 219.62.

Additionally, two rings of thirty-two pressure taps were installed on the afterbody plug at FS 219.3 and 249.3 to measure surface pressure distribution aft of the radome.

Wind Tunnel Facility & Test Conditions

The test was conducted at Langley Full Scale 30ft X 60ft Wind Tunnel, operated by Old Dominion University.

As illustrated in Figures 1and 2, the model was attached to a hydraulically actuated model support that generated vertical pitch motion, which provided up to 62° angle of attack for this test. The model support was mounted to the turntable mechanism on the ground board. The rotation of the turntable combined with the pitch motion of the model support system produced flexible angle of attack and angle of sideslip combinations for the model.

The baseline wind tunnel test speed was set at a dynamic pressure of 10 psf. The corresponding test velocity was 92 ft/sec with Reynolds number reaching nearly 0.6×10^6 ft^{-1}.

Although the balance's moment center was located at FS 219.62, WL116.173, and BL 0, the data acquisition/reduction system was configured to resolve all moments to the F-15's Aerodynamic Reference Point at FS 557.173, WL 116.173 and BL 0. All force and moment data presented in this document are in the body-axis system and are relative to the Aerodynamic Reference Point. Furthermore, all aerodynamic coefficients were calculated based on the standard F-15 dimensions with S = 608 ft^2, MAC = 15.94 ft and b = 42.8ft.

Because the six component force and moment data were acquired using only the first of 12 ft of the F-15 forebody, the resulting aerodynamic data were expected to be lower in magnitude due to the absence of the remaining forebody. Nevertheless, the characteristics of these data is representative of the forebody's contribution to the overall F-15's aerodynamic characteristics in the high angle of attack region where previous component tests (*e.g.*, Ref. 6) have shown the forebody to dominate the yaw characteristics.

Pressure Data

Consistent with conventional static pressure representation, the measured local static pressure values were nondimensionalized by the test section's dynamic pressure to arrive at the local pressure coefficient Cp.

$$Cp_{local} = (P_{local} - P_\infty) / Q_\infty.$$

The pressure coefficient values were assigned to a color spectrum and mapped over the surface of the forebody to allow visualization and comparison of the entire region's surface pressure distribution. This technique permitted intuitive and rapid evaluation of local surface flow conditions. As shown in the example in Figure 3, the color contour on the forebody was mapped according to the pressure spectrum. Regions of orange, red and magenta represent increasing suction, while areas with shades of green and blue indicate positive pressure. The intersections of the gridlines identify the locations of the pressure ports on the forebody. As seen in Figure 3, the view point for most pressure plots presented in this report is equivalent to positioning the eye point in front of the radome and looking directly at the forebody. This

perspective is necessary to permit easy contrast of the pressure variations between the two sides of the forebody when examining forebody asymmetric flow phenomenon. One must also keep in mind that the colored region represents an area nearly 11 ft in length as shown on the side view in Figure 4.

Discussion Of Test Results

Baseline Characteristics

The yawing moment comparison as a function of angle of attack for the two production radomes examined at 0°β is shown in Figure 5. As the angle of attack increased above 45°α, a small positive yawing moment was developed for both the tapped (R1) and untapped (R2) foerbodies. This yawing moment offset continued to increase with angle of attack, which was a direct result of the imbalance of surface pressure distribution between the left and right sides of the forebody, evident in Figure 6.

At high angles of attack, the pressure plots show how the airflow accelerates around the nearly circular cross-section, and as a result, a low-pressure region was produced on the sides of the forebody. With increasing angle of attack, the stagnation region, as outlined in the blue area, migrated downward from the apex to the bottom of the forebody. As the flow accelerates around the two sides of the forebody, low-pressure regions develop. On each side of the forebody, this favorable pressure gradient becomes more pronounced with increasing angle of attack, and the development of the suction region is enlarged. Slowing down in the abrupt adverse pressure gradient toward the upper quadrant of the forebody, the flow separates off the forebody. Following separation, the flow rolls up into an off-surface vortex, evidenced above 50°α by the pair of faint vortex tracks on the upper surface of the forebody starting at the apex. In this case, the slightly greater suction region on the right side of the F-15 forebody produces a net positive side force and results in a positive yawing moment about the Aerodynamic Reference Point.

Sideslip Effects

A comparison of the directional characteristics for the two production radomes is shown in Figure 7. Through 45°α, both radomes exhibited linear variation in yawing moment with increasing sideslip angle as evident in the constant slope of yawing moment coefficient with angle of sideslip. Above 50°α, the effects of the mild yawing moment asymmetry at zero-sideslip could be seen propagated to sideslip angles as high as ±10°β. However, by ±20°β, the effect of the flow asymmetry had dissipated.

Effects of Forebody Surface Imperfections

The survey of the radome cap conditions on the F-15 fleet conducted by McDonnell Douglas revealed that a wide variety of surface imperfections may occur after the aircraft entered service. On the steel cap alone, they included surface paint erosion and peeling, misalignment with the radome apex, gaps at the trailing edge, extruded sealant near the cap trailing edge, and even flat spot cap deformation. This section documents the various radome nose cap imperfections examined in the wind tunnel and their corresponding aerodynamic characteristics.

Nose Cap Roll Orientation-Painted Cap

During the model construction, the nose cap was removed from the tapped forebody to allow the removal of the rain erosion boot for the pressure port installation. Before the start of the test entry, the cap was visually inspected for any obvious signs of geometric anomalies before it was reinstalled.

After the baseline characteristics were collected for the tapped radome, the nose cap was again removed to allow testing of other configurations. However, later check runs revealed noticeable differences in yawing moment characteristics at high angles of attack before and after the re-installation of the same nose cap. Repeat runs indicated the variations in the yawing moment characteristics were not the results of improperly installed nose cap, and that no other visually detectable imperfection could be seen on the nose cap other than a minute mark (1/8-in. x 1/32-in.) on the nose cap surface near the trailing edge. At that time, a decision was made to quantify the variability in yawing moment offset by testing with the baseline nose cap set at different roll orientations using the existing mark as a reference.

The results of this test series are summarized in Figure 8. By changing the nose cap's roll orientation, the yawing moment characteristics ranged from +0.013 to -0.005 at 62°α. Also note that a measurable yawing moment offset was detected for certain configurations at as low as 37.5°α. While it was unclear whether these variations were a direct result of the mark or the potentially uneven distribution of the residual sealant on the back side of the nose cap, the variability on the yawing moment at moderate and high angles of attack highlighted the flow's extreme sensitivity to minute geometric variations at the apex of the forebody. Once the roll orientation of the nose caps was clearly identified, subsequent repeat check runs yielded consistent offset characteristics.

Nose Cap Roll Orientation-New, Unpainted Cap

A new, unpainted radome nose cap was provided by McDonnell Douglas. Following the discovery of the yawing moment offset's sensitivity to the painted nose cap's roll orientation, a series of runs

were performed to determine if the same observation could be made for a new unpainted cap.

An ink mark was made on the trailing edge of the new nose cap using a permanent marker to identify the new cap's roll orientation. The yawing moment offset characteristics of the new cap at four different roll orientations are shown in Figure 9. With the yawing moment asymmetry spanning ±0.005 at high angles of attack, the magnitude of the offset for the new unpainted cap was considerably less than that for the original painted nose cap. Furthermore, in contrast with the data taken for the painted cap, the onset of the yawing moment asymmetry was delayed to higher angles of attack (50°α vs. 35°α) with the new nose cap.

Nose Cap Anomalies

The survey of conditions on the fleet F-15's prior to the test revealed several cases of symmetric and asymmetric paint erosion on the nose cap resulting in a build up of paint layers at the trailing edge of the cap. To simulate asymmetric paint loss on the nose cap, a layer of ¼-in. wide by 1/16-in. thick clay with enough length to cover ¼ circumference of the nose cap was applied as illustrated in Figure 10. The positions of the simulated paint ridge were varied to determine their effects on the yawing moment characteristics

In addition to the paint erosion noted above, a 1/8-in. gap at the trailing edge of the nose cap was observed on an F-15 at Langley AFB (Figure 11); a result of an uneven application of sealant under the nose cap during installation. This imperfection was modeled in the wind tunnel by applying 1/8-in. layer of clay between the nose cap and the radome surface. The location of the resulting cap gap was varied to determine the most sensitive configuration.

The yawing moment characteristics for these configurations are summarized in Figure 12. The effect of paint erosion was seen to be highly dependant on the location of the simulated paint ridge, with the aerodynamic effects ranging from symmetric to large positive yawing moment offset.

The yawing moment asymmetry corresponding to the cap gap configurations are compared in Figure 12. Significant yawing moment offset was observed for the left cap gap configuration. For this cap gap configuration, the asymmetry was detected at as low as 40°α. The positive yawing moment offset increased almost linearly with the angle of attack and reaches the maximum value of +0.0195 at 62°α.

The forebody surface pressure distribution responsible for the cap gap yaw asymmetry at 62°α is shown in Figure 13. The regions of strong negative pressure are highlighted by the white color band. Because of the cap gap imperfection, earlier separation was induced, and the suction region on the left side of the forebody was reduced while the suction area on the right side of the forebody was increased. This significant imbalance of pressure distribution between the left and right sides of the forebody resulted in the net positive side force and ultimately positive yawing moment about the aerodynamic reference point.

Also note that the pressure differential propagated throughout the length of the forebody model. This would indicate that a greater magnitude in yawing moment offset would be expected for the full scale F-15 configuration given that the remainder of the forebody and canopy would provide additional surface areas for this pressure differential to act on.

Having generated the greatest yawing moment offset, the lower-left cap gap configuration was tested under sideslip conditions. Figure 14 compares the cap gap's directional characteristics against the baseline R1's directional characteristics. At low angles of attack, the imperfection had no effect. However, as the angle of attack increased, the left cap gap caused a positive yawing moment offset, especially at positive sideslip angles. Comparing the yawing moment above 40°α, the effect of the left cap gap grew more pronounced with increasing positive sideslip angle and diminished with greater negative sideslip. Above 55°α, the yawing moment offset was sufficiently large to overcome the natural directional characteristics of the forebody and resulted in a positive yawing moment displacement through +20°β.

The forebody surface pressure distribution comparison between the lower-left cap gap and the baseline configurations at large sideslip angles are shown in Figure 15. At -20°β, the stagnation region on the left side of the forebody combined with the large suction area on the right side of the radome produced a net positive yawing moment. Consistent with the yawing moment characteristics shown in Figure 14, there was no noticeable difference in forebody pressure distribution between the baseline and the cap gap configuration at -20°β. On the other hand, the cap gap configuration had a significantly greater effect at +20°β. At positive sideslip angle, although the stagnation region on the under side of the forebody was unaffected, the cap gap configuration was able to increase the suction area on the right side of the forebody, and trigger a reduction in the suction region on the left side of the radome resulting in a net positive yawing moment.

In order to determine whether this yawing moment offset was caused by the asymmetric surface discontinuity at the cap trailing edge or the misalignment of the nose cap, the 1/8-in. left cap gap was faired by applying clay to the region behind the cap's trailing edge as illustrated in Figure 16. As shown in Figure 17, when the 1/8-in. gap at the cap's left trailing edge was

eliminated with the fairing, leaving only a significantly smaller step on the right trailing edge of the cap, a negative yawing moment offset was produced. Although slightly smaller in magnitude than the previously tested gap, the small right gap produced a -0.015 yawing moment offset at 62°α. When the clay fairing was applied completely around the trailing edge of the nose cap as shown Figure 16, no yawing moment asymmetry was observed.

The forebody pressure distribution plot comparing the two faired configurations against the baseline cap gap at 62°α is shown in Figure 18. Clearly, the elimination of the 1/8-in. deep surface discontinuity on the left and leaving only a small step at the cap's right trailing edge had completely reversed the direction of the asymmetry. Further, completely fairing the misaligned cap's trailing edge discontinuity resulted in symmetric suction on the sides of the forebody. These results indicated that the misalignment of the nose cap alone did not generate forebody flow asymmetry, rather, the observed behavior arose from the asymmetric surface discontinuity caused by the tilted cap's trailing edge. The data collected on the various nose cap imperfections had clearly demonstrated that the forebody flow field's extreme sensitivity to the conditions on the nose cap.

Bumps on Rain Erosion Boot

Many F-15 radomes in service are fitted with a 14-in. long rain erosion boot that starts from under the nose cap at the apex of the radome. The pre-test inspection of the fleet radomes had observed some bubbles and bumps on the rain erosion boot (see Figure 19) due to pockets of trapped air and possibly uneven distribution of sealant under the boot surface. Several configurations to model these bumps were tested.

A report of right yaw departures at high angles of attack for F-15 No. 3042 at Langley AFB at the start of the wind tunnel entry prompted an immediate inspection of its radome. A ½-in. long, 1/8-in. tall bump was observed on the left side located at ½ in. behind the nose cap's trailing edge as previously shown in Figure 11. A clay bump with similar dimensions was applied to the R1 radome to simulate the 3042 bump. Testing revealed the bump produced a moderate yawing moment offset above 50°α as seen in Figure 20.

A 0.5-in. tall, 1.2-in. diameter circular bump was positioned on the upper-left quadrant 1.5-in. behind the cap's trailing edge. This medium-size bump consistently produced significant yawing moment asymmetry above 50°α reaching a maximum value of +0.0185 of Cn at 62°α as shown in Figure 20. In order to correlate the magnitude of the yawing moment offset obtained for the 12-ft forebody to the yawing moment characteristics scaled from a 10%-scale F-15 model with a forebody bump (Ref. 8), a large bump (2.6-in. diameter, 1.6-in. high located at FS120.3) was applied to the scaled test location. As shown in Figure 20, this large bump configuration generated yawing moment asymmetry at as low as 35°α and continued to increase with higher angles of attack.

Note that other than the slightly greater onset of the asymmetry below 45°α, the yawing moment characteristics for the large bump configuration very closely matched those obtained for the lower-left cap gap configuration. This suggested both configurations had triggered the maximum yawing moment offset attainable for the forebody model without additional gross geometric changes to the forebody. Further, aerodynamic characteristics extracted from the Keep Eagle program's flight data indicated the F-15E exhibited a peak asymmetric yawing moment coefficient approaching +0.03 at 60°α (Ref. 7). Both the 10% low-speed static test and the 9%-scale rotary balance data for the whole F-15 configuration showed a yawing moment coefficient offset approaching +0.037 at 65°α (Ref. 5 and 8). Therefore, correlating the maximum forebody offset value from this test series to the full-configuration F-15 aircraft would require an approximate scaling factor of 1.5 to 2.0.

Conclusions

The force and moment measurement as well as pressure data collected from this full-scale F-15 forebody test clearly demonstrated significant side force and yawing moment asymmetry can be generated by very small geometric imperfections near the radome's apex. Minute nose cap anomalies such as a trailing edge gap, flat spot, extruded sealant, and uneven paint erosion can trigger significant directional offset at moderate and high angles of attack. The resulting asymmetric flow phenomenon is robust enough to diminish or even overcome the effects of sideslip as high as 20°. Further, if located near the tip of the forebody, bumps on the rain erosion boot area can induce substantial directional asymmetry similar in magnitude to those caused by the nose cap imperfections. In contrast, radome damages and repair patches located further aft on the radome, unless grossly exaggerated, had minimal effects on high angle of attack yawing moment characteristics.

An inferred conclusion from this full-scale test suggests that innovative control concepts designed to exploit the manipulation of the forebody boundary layer at the apex of the nose should require smaller inputs than earlier subscale testing had indicated. Further, the repeatability of the results also indicates that these controllers' robustness may be greater than what previous subscale results have suggested. For forebody pneumatic blowing controllers, mass flow requirements may be significantly reduced if the jets were properly positioned near the forebody apex.

References

1. Pauley, H., Ralston J. and Dickes E.: "Experimental Study of the Effects of Reynolds Number on High Angle of Attack Aerodynamic Characteristics of Forebodies During Rotary Motion." NASA CR 195033, January 1995.
2. Keener, E. R., and Chapman, G.T.: Onset of Aerodynamic Side Forces at Zero Sideslip on Symmetric Forebodies at High Angles of Attack, AIAA 74-770, August 1974.
3. Lamont. P. J.: Pressure Measurements on an Ogive Cylinder at High Angles of Attack with laminar, Transitional or Turbulent Separation, AIAA 80-1556, August 1980.
4. Hall, R. M: Influence of Reynolds Number on Normal and Side Forces on Ogive Cylinders at High Incidence, AIAA 85-1799 August 1985.
5. Traven, Ricardo: "Bridging the Gap: One Attempt to Transfer Ideas from X-Plane to Airplane to Improve High AOA Handling Qualities." High-AOA Technology Conference, Sept. 1996.
6. Kay, J. and Ralston, J.: "F-15E High Angle of Attack Study, Including Data, Analysis, Aerodynamic Math Modeling and Simulation." BAR95-2. March 1995.
7. Peters, G.: "F-15 Keep Eagle Program TCM Flight Test Results – Parameter Identification (Part 2)." MDA. Sept.11, 1995.
8. Undocumented 10%-scale F-15 test at NASA Langley. May, 1994. Test No. LaRC 052.

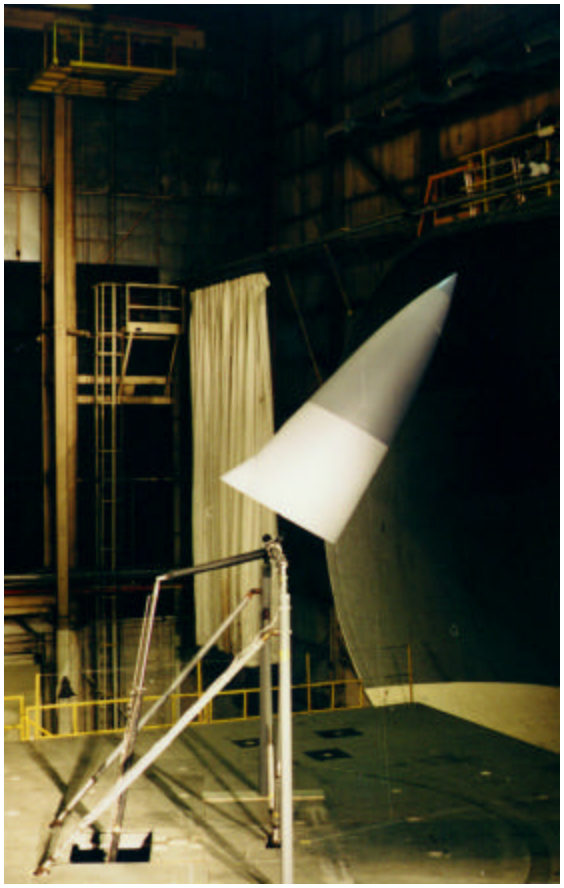

Figure 1 F-15 Radome in the Langley 30x60 Full Scale Test Section.

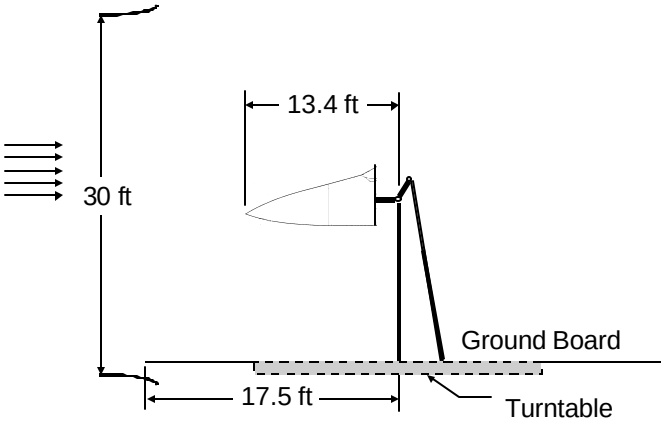

Figure 2. F-15 forebody with model support, ground board and turntable.

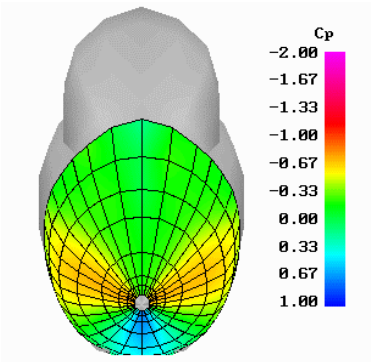

Figure 3 Forebody tap and surface pressure distribution.

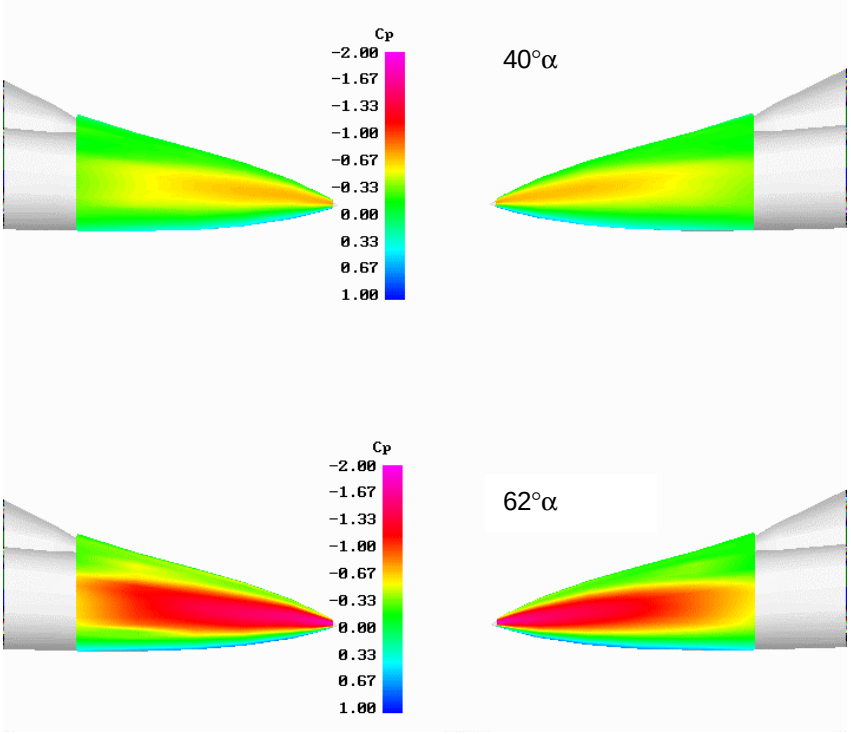

Figure 4. Side view of forebody pressure distribution.

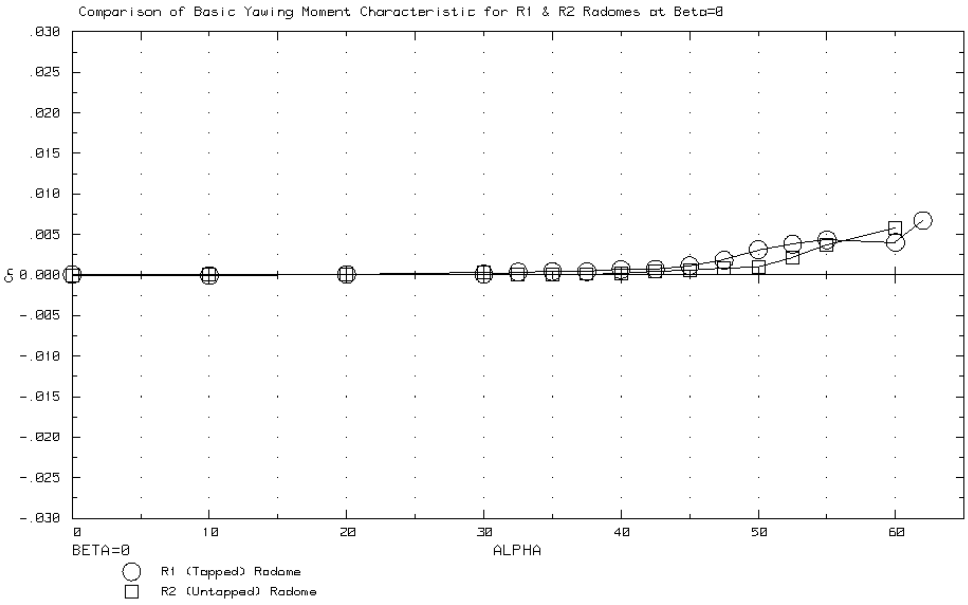

Figure 5. F-15 forebody yawing moment at 0°β.

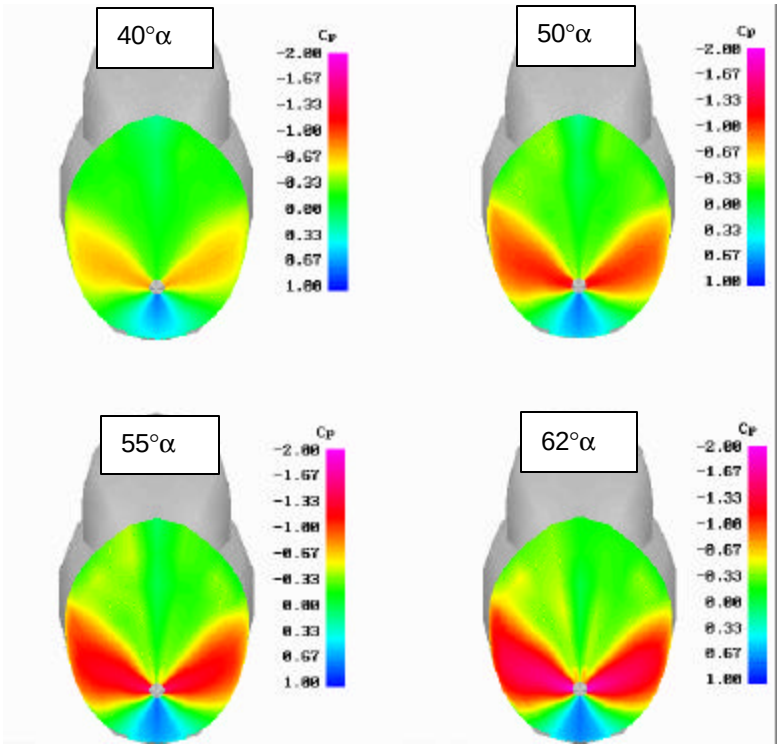

Figure 6. Pressure distribution on baseline forebody.

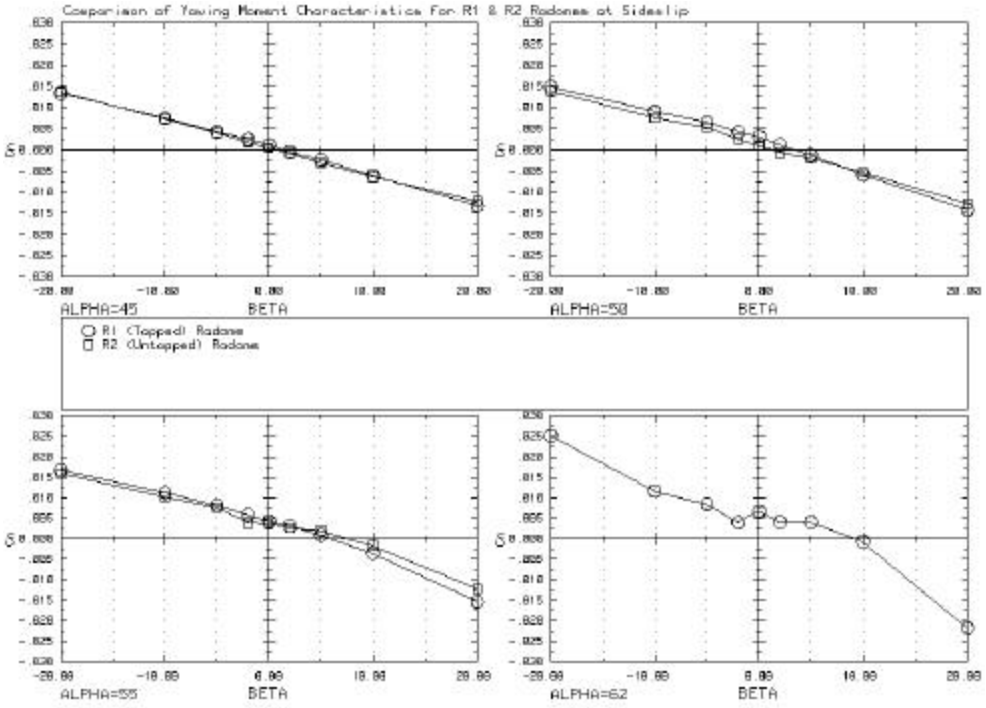

Figure 7. Effect of sideslip on tapped (baseline) and untapped production radomes.

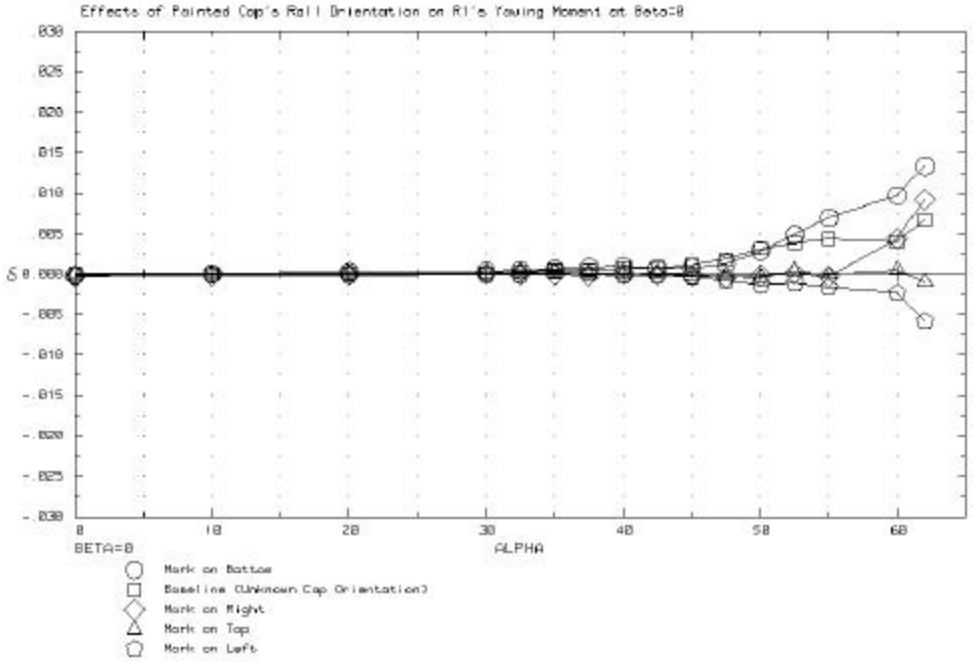

Figure 8. Effects of painted cap's roll orientation on yawing moment at 0°β.

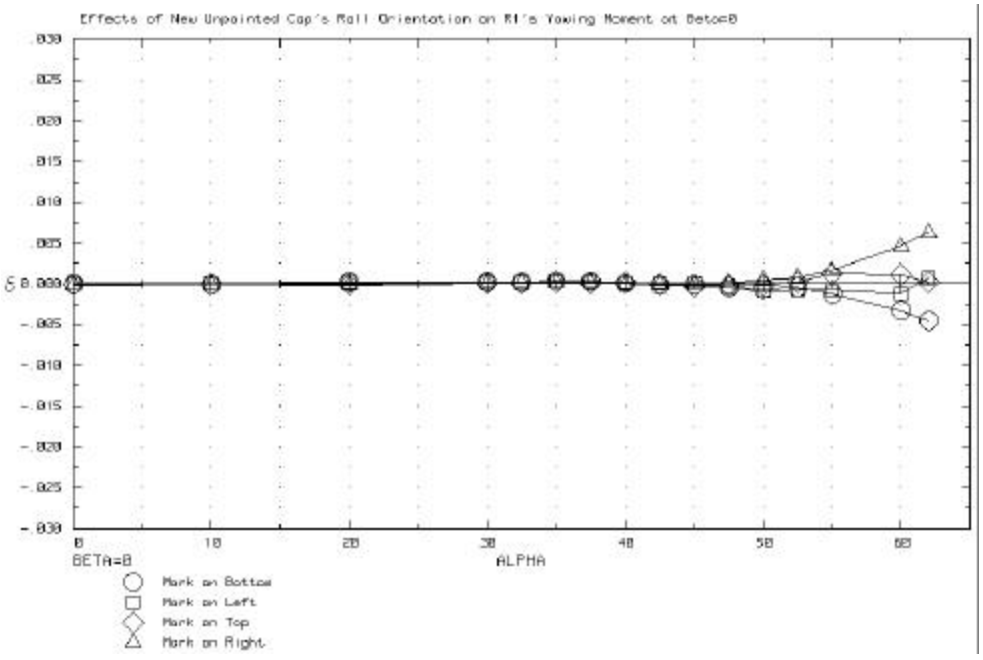

Figure 9. Effects of new unpainted cap's roll orientation on yawing moment coefficient at 0°β.

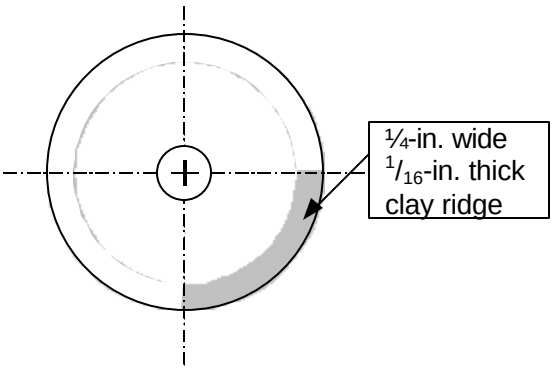

Figure 10. Simulated paint ridge on nose cap.

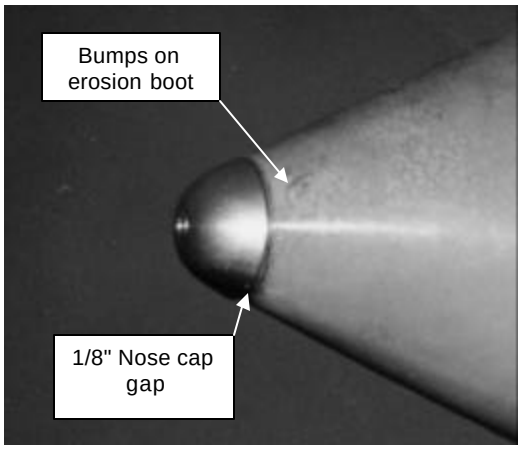

Figure 11. Imperfections observed on Langley F15C 3042.

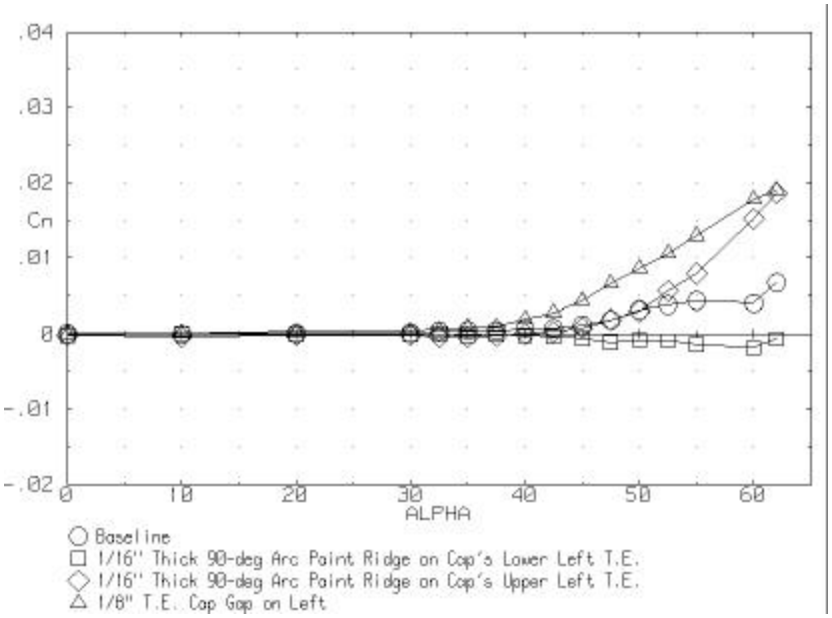

Figure 12. Effect of nose anomalies on forebody yawing moment

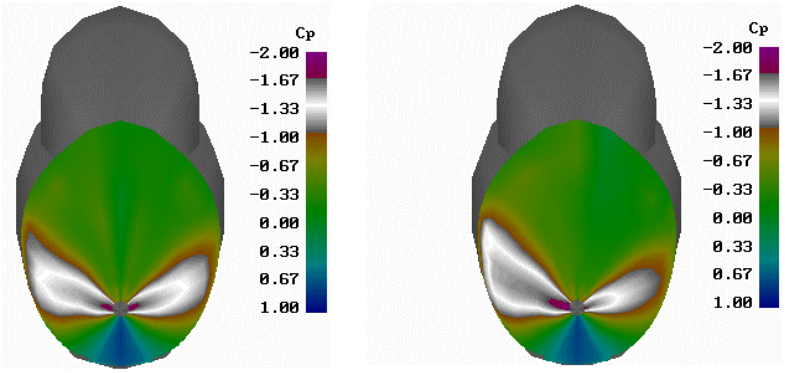

Figure 13. Effect of nose cap gap on forebody pressure distribution.

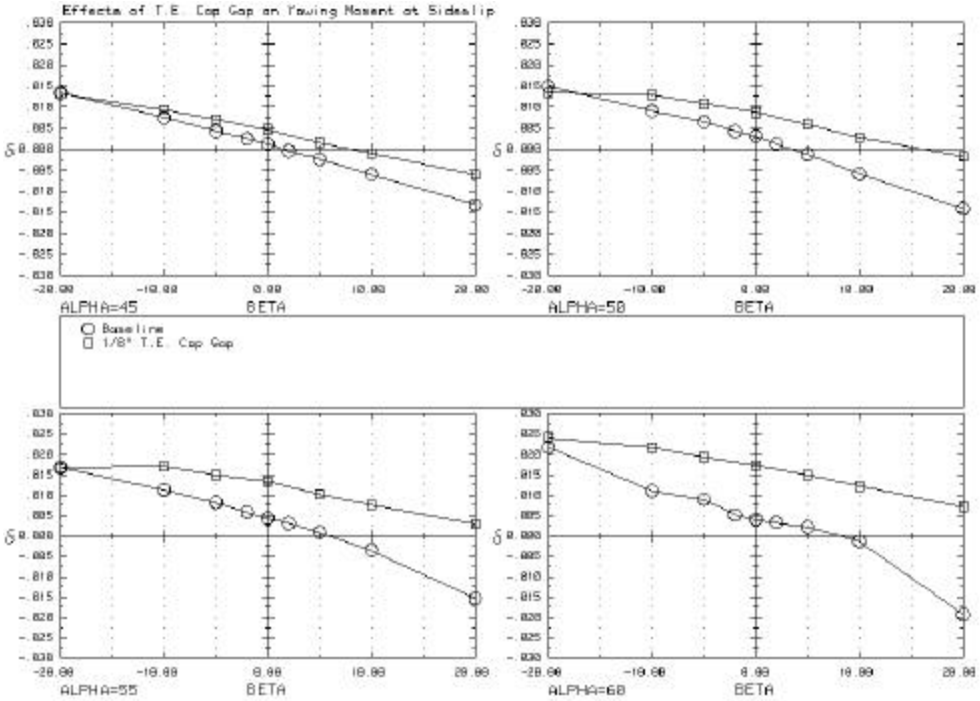

Figure 14. Effect of nose cap gap on yawing moment at sideslip.

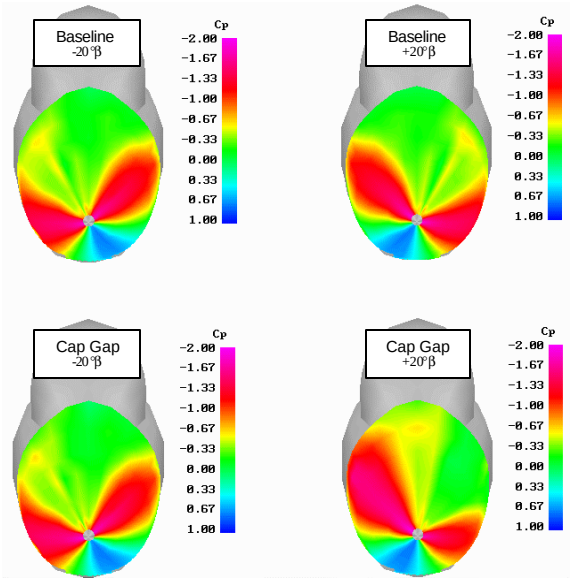

Figure 15. Effects of nose cap gap at sideslip on forebody pressure distibution.

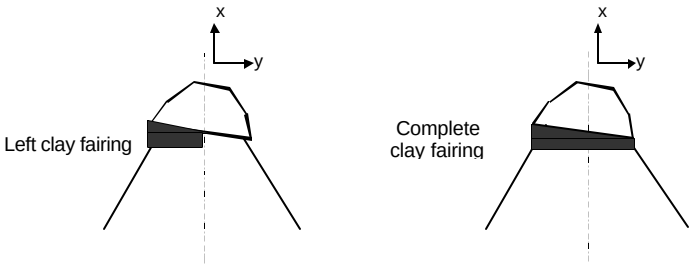

Figure16. Clay fairing of misaligned nose cap.

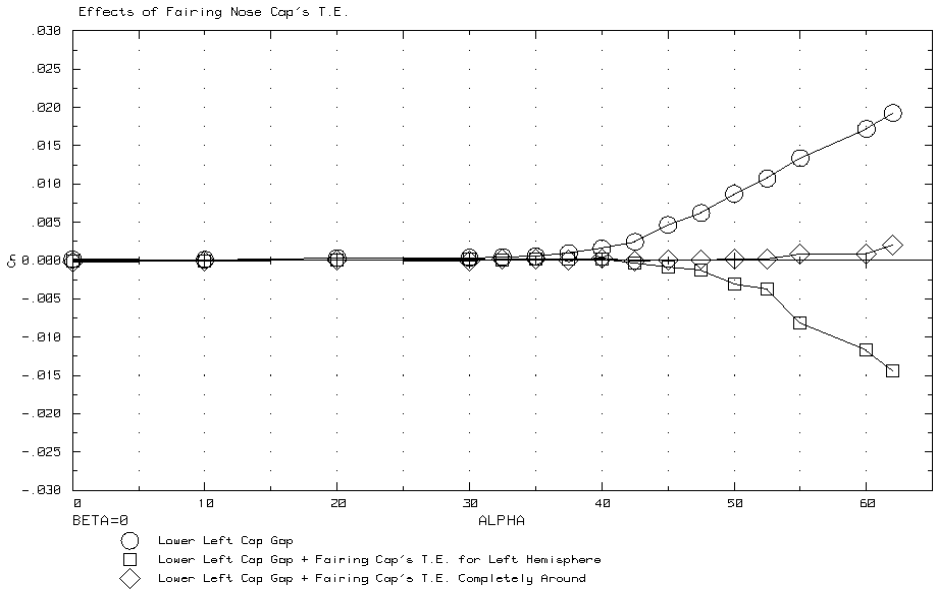

Figure 17. Effects of clay fairing of misaligned nose cap.

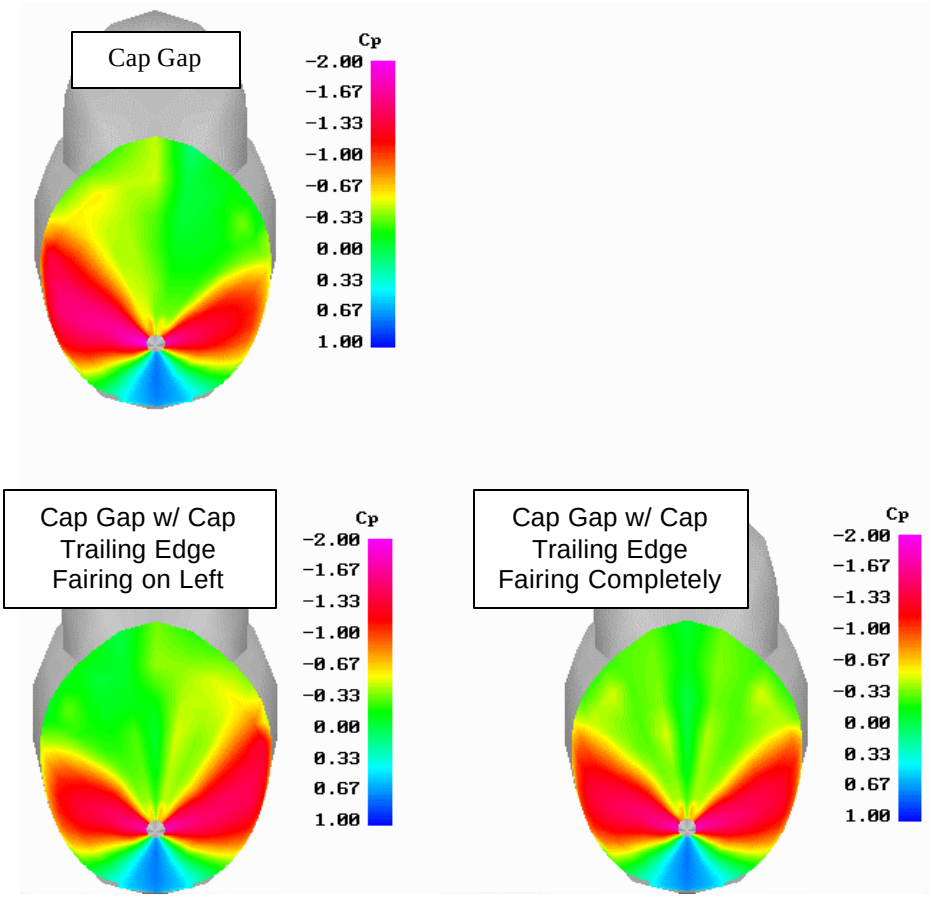

Figure 18. Effects of clay fairing on forebody surface pressure distribution.

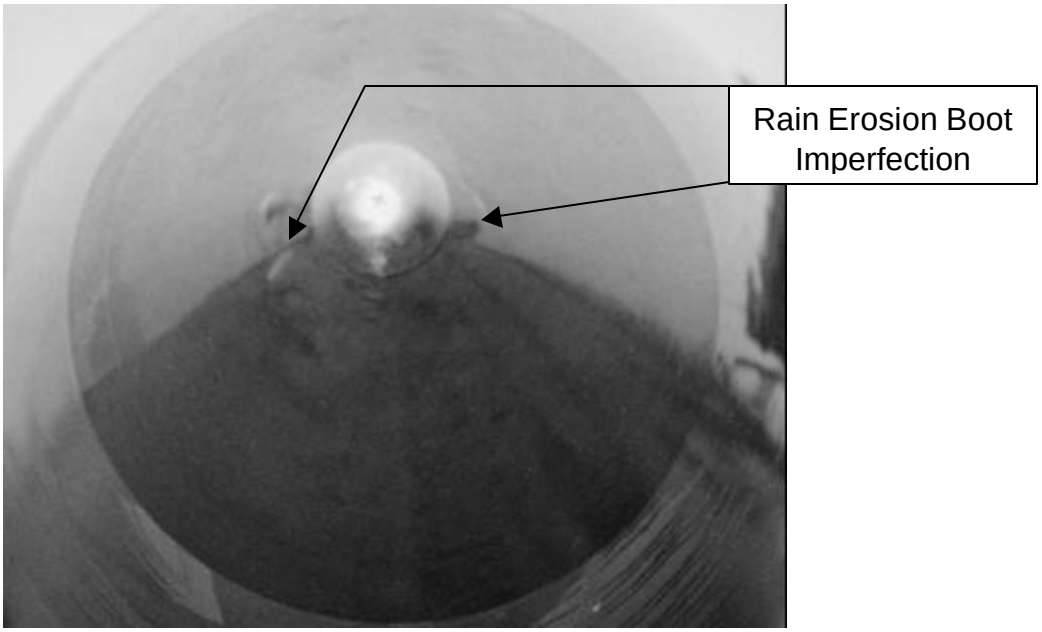

Figure 19. Typical rain erosion boot imperfections.

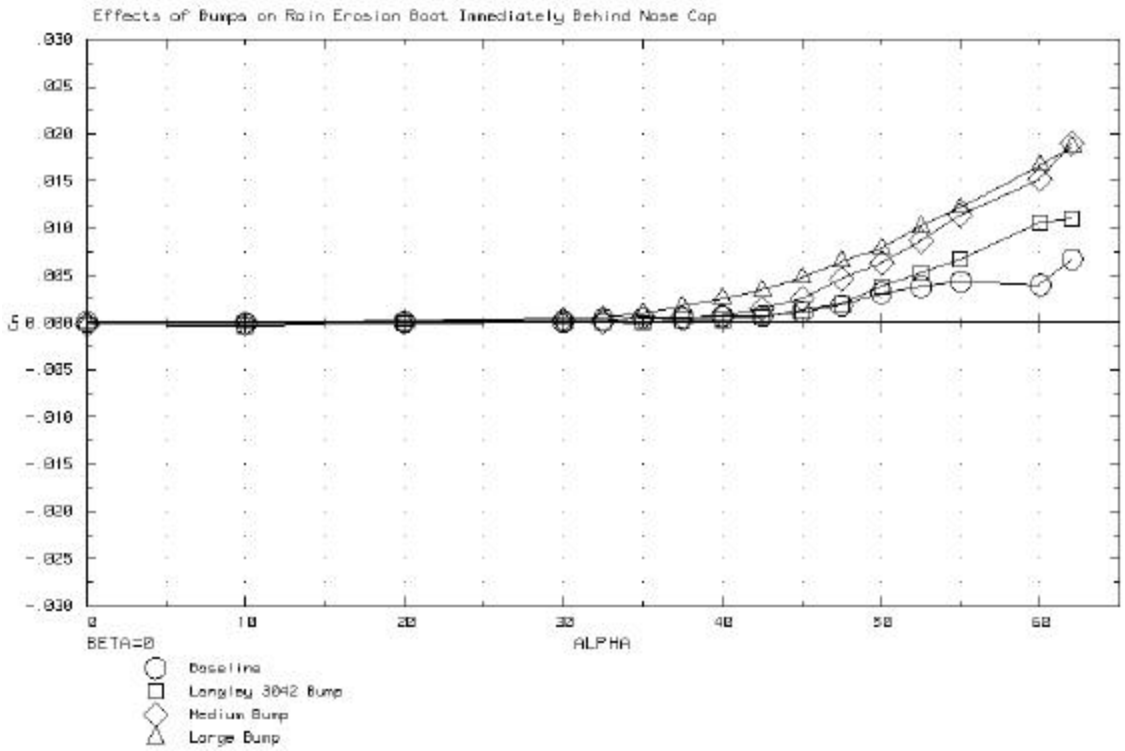

Figure 20. Effect of forebody bumps on yawing moment